NASA TECHNICAL NOTE

NASA TN D-3631

NASA TN D-3631

DETERMINATION OF TEMPERATURE AND MATERIAL EFFECTS ON HIGH-VELOCITY IMPACT CRATERS IN ABLATIVE HEAT-SHIELD MATERIALS

by Paul E. Tippens and John R. Davidson

Langley Research Center
Langley Station, Hampton, Va.

NATIONAL AERONAUTICS AND SPACE ADMINISTRATION • WASHINGTON, D. C. • SEPTEMBER 1966

NASA TN D-3631

DETERMINATION OF TEMPERATURE AND MATERIAL EFFECTS ON HIGH-VELOCITY IMPACT CRATERS IN ABLATIVE HEAT-SHIELD MATERIALS

By Paul E. Tippens and John R. Davidson

Langley Research Center
Langley Station, Hampton, Va.

NATIONAL AERONAUTICS AND SPACE ADMINISTRATION

For sale by the Clearinghouse for Federal Scientific and Technical Information
Springfield, Virginia 22151 – Price $1.00

DETERMINATION OF TEMPERATURE AND MATERIAL EFFECTS ON HIGH-VELOCITY IMPACT CRATERS IN ABLATIVE HEAT-SHIELD MATERIALS

By Paul E. Tippens and John R. Davidson
Langley Research Center

SUMMARY

Phenolic-nylon and elastomeric target materials were struck with 1.59-mm-diameter aluminum spheres traveling at 4 km/s. The ablative materials were tested at temperatures of 144°, 294°, and 422° K in evacuable test fixtures. Observed crater volumes were so irregular in shape that it was not possible to determine easily the effects of temperature and material independently from measurement error. Therefore, an analysis-of-variance technique was applied to experimental impact data to determine whether differences in material or temperature significantly affect the amount of crater damage. It was found in this investigation that no significant differences among the crater diameters or the penetration depths were attributable to temperature differences. However, both crater depth and diameter were influenced by differences in target materials.

INTRODUCTION

Space vehicles which are to survive atmospheric entry must be protected by heat shields. The purpose of a heat shield is to reduce the heat input to the vehicle structure. Ablative materials are frequently used because they generally provide the most efficient thermal protection system.

Because heat shields are usually exposed to the space environment for indefinite periods during orbit or space travel, these shields are susceptible to damage by impacting meteoroids. Near the vicinity of the earth meteoroids travel at speeds from 11 to 71 km/s; at such speeds even small particles can cause a crater of appreciable size in ablative plastic materials.

The purpose of this series of tests was to ascertain whether material temperature and/or composition had any effect on the size of the crater caused by a hypervelocity particle. The temperature range selected was from 144° K to 422° K, because this range covers the expected temperature range of an exposed heat shield in a space environment.

Unfortunately, meteoric speeds are extremely difficult to attain in the laboratory with projectiles of finite mass. A test velocity of 4 km/s, however, could be obtained consistently with a light-gas gun, and this velocity was used in all tests. A 1.59-mm-diameter aluminum sphere was used as the projectile.

SYMBOLS

The units used for the physical quantities defined in this paper are given in the International System of Units (SI). See reference 1.

b	minimum momentum per unit area necessary to produce a penetration, kilograms/meter-second
d	projectile diameter, meters
E	modulus of elasticity of target material, newtons/meter^2
F	sampling distribution for testing hypotheses
m,n	number of observations in each mean
N	total number of measurements
P	penetration depth, meters
R_S	residual sum of squares
r,k	number of rows and columns, respectively
SS_r	sum of squares in row
SS_k	sum of squares in column
T_S	total sum of squares
$T_{i.}$	sum of all observations in the ith row
$T_{.j}$	sum of all observations in the jth column

$T_{..}$ sum of all of the observations

t thickness, meters

V projectile velocity, meters/second

ρ density, kilograms/meter^3

α population variance

Subscripts:

i,j indices

p projectile

cr critical

min minimum

Superscript:

* mean square

APPARATUS

Targets and Projectiles

The target materials tested were representative of materials which might be used in ablative heat shields. The base materials were phenolic-resin and silicone elastomers. In combination with these materials, nylon powder, phenolic-Microballoons (hollow spheres of phenolic resin), Eccospheres (hollow silica spheres), and phenolic-honeycomb were used to obtain various densities and degrees of reinforcement in the targets. The compositions of the target materials are identified in table I, where the five different target materials are designated A to E.

Disk-shaped targets were machined from the composite materials listed in table I. The diameter of the disks was dictated by the internal dimensions of the test facilities described subsequently. The target thicknesses were determined in such a manner that

the total mass per unit area was the same for all materials: 19.6 kg/m^2, which is in the range of typical heat-shield area densities.

Target disks, each containing a copper-constantan thermocouple, were insulated from the target holders with cylindrical spacers of acetate foam. The specimen, spacer, and holder were bonded with a high-temperature epoxy resin, and each specimen was painted with a thin coat of black paint to increase the radiant heat transfer between the specimen and the target-chamber walls.

Preliminary calculations were made to determine a projectile size and material such that complete penetration would not occur in any of the target specimens.

A study of impact into metal and plastic targets is reported in reference 2. The depth of penetration was found to be related empirically to the momentum per unit area of the projectile in the following manner:

$$P = \frac{622\left(\rho_p V d - b\right)}{\rho_p{}^{.278}\left(E + 1.93 \times 10^{10}\right)^{.78}} \tag{1}$$

In equation (1) the depth of penetration P is in meters, the density of the projectile ρ_p is in kg/m^3, the velocity V is in m/s, the modulus of elasticity of the target material E is in N/m^2, and the projectile diameter d is in meters. The parameter b is a material strength parameter; if the momentum per unit area is less than b, no penetration occurs. In the case of nonmetals, b is negligible with respect to the values of $\rho_p V d$ used in the present investigation.

Equation (1) was chosen because it was originally obtained as an empirical "fit" to results of hypervelocity-impact tests which included plastic targets. The required values of E for the materials described in the present report were measured by compression tests in a standard hydraulic compression testing machine.

Reference 3 indicates, at least for metals, that thin sheets will be completely penetrated if their thickness is less than $1.5P$, where P is calculated from equation (1). Accordingly, the minimum acceptable target thickness was obtained by multiplying the right-hand side of equation (1) by 1.5, to obtain

$$d = \frac{1}{\rho_p V} \frac{t_{min}\rho_p{}^{.278}\left(E + 1.93 \times 10^{10}\right)^{.78}}{1.5(622)} + b \tag{2}$$

An existing light-gas gun was used to launch the projectiles; the maximum consistent velocity obtainable with this gun is 4 km/s. The substitution of this value for velocity into equation (2), together with the elasticity data from table II yields a maximum

aluminum projectile diameter of 1.59 mm. A larger projectile might be expected to penetrate targets composed of material A.

Experimental Facilities

The general hypervelocity range test apparatus arrangement is shown schematically in figure 1. The target test chambers were mounted at one end of the hypervelocity test range.

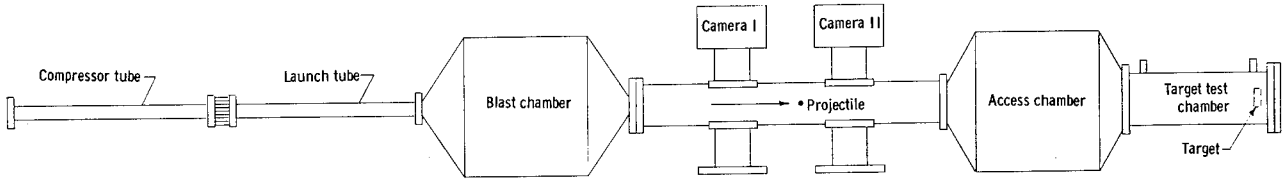

Figure 1.- Hypervelocity test range apparatus showing location of the light-gas gun, range instrumentation, and target test chamber.

High-temperature test chamber.- The high-temperature target test chamber was a cylindrical, double-walled, steel vacuum chamber approximately 66 cm long. A sketch of a section along the length of the chamber is shown in figure 2. The outer sleeve was

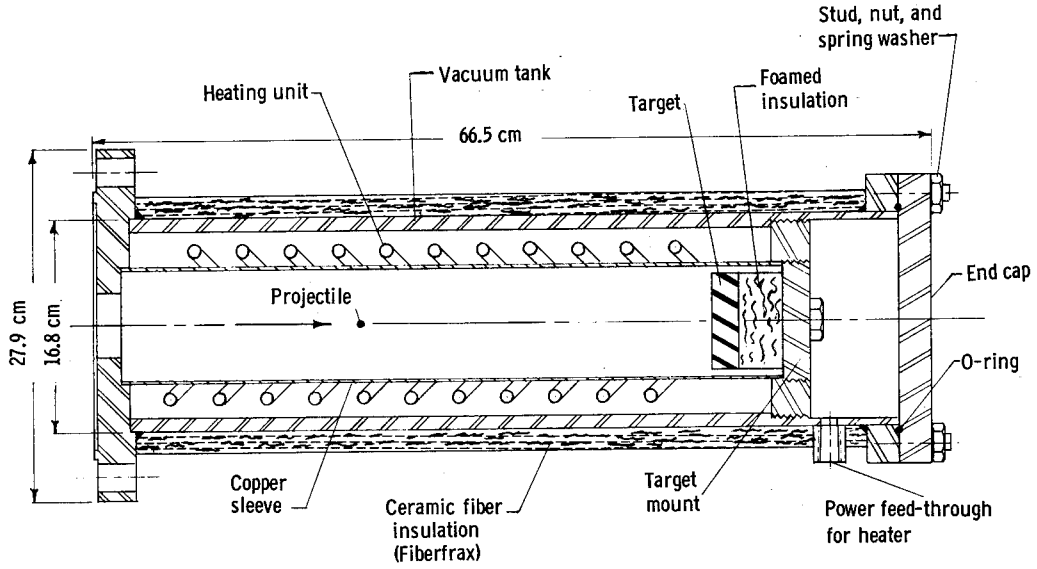

Figure 2.- High-temperature test chamber. The projectile entered hole in left end and struck target at right. The extended instrumentation-lead feed-through pipe is not shown.

designed to be pressure tight. The inner sleeve was a rolled sheet of copper inserted inside the helical heating unit; the purpose of the inner sleeve was to insure even distribution of radiant heat to the target. The 4500-watt capacity of the heating unit was ample to raise the target to the maximum test temperature of 422° K in about 30 minutes. Vacuum fittings were used to permit thermocouple wires to be attached to an external temperature recorder so that the target temperature could be monitored continuously.

During a test the target chamber was mounted to the end of the hypervelocity test range apparatus (see fig. 1); the connection between the access chamber in the hypervelocity test range apparatus and the target chamber was sealed by means of an O-ring. The connecting bolts (and also the bolts holding the end caps to the target chambers) used spring washers to compensate for thermal expansion or contraction. The projectile entered the target chamber through a hole in one end and struck the target, which was mounted on a removable threaded target mounting disk at the other end. The target was insulated from the mounting disk by a layer of foamed plastic; this arrangement prevented large temperature gradients in the target which otherwise would have been caused by heat conducted through the metal mounting disk.

Although not utilized during this test series, the maximum operating temperature of the hot chamber is 813° K; this temperature is governed by the brazing alloy used on the inner sheet.

Low-temperature test chamber.- A sketch of the low-temperature aluminum test chamber is shown in figure 3. Again, this cylindrical chamber was of double-wall

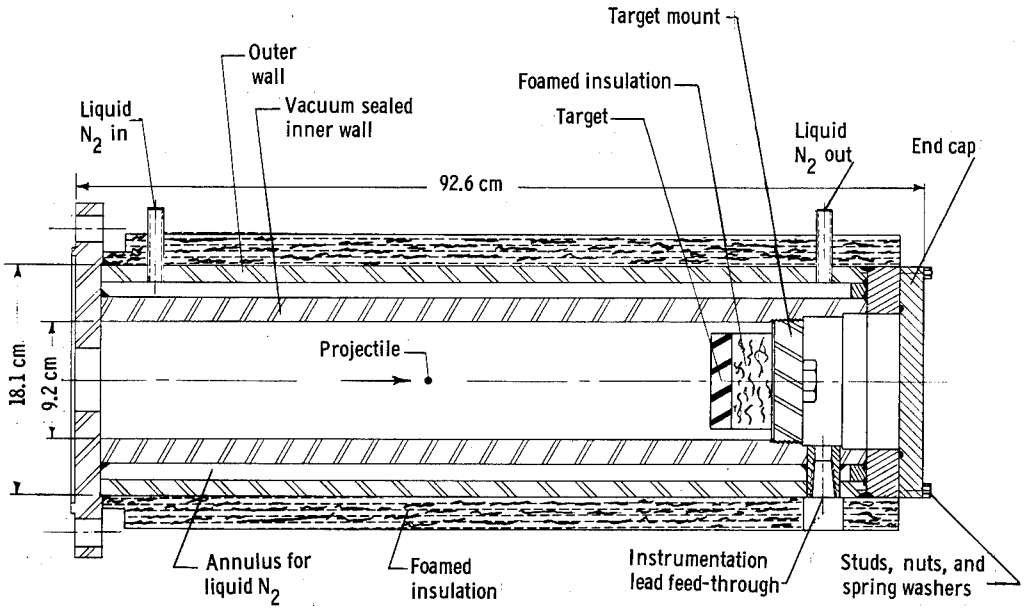

Figure 3.- Low-temperature test chamber. The projectile entered hole in left end and struck target at right end.

construction, approximately 64 cm long, but in this case the inner wall was constructed to be vacuum tight. The low temperature was obtained by pouring liquid nitrogen between the walls. In order to reduce the need for large amounts of liquid nitrogen, the outer wall was insulated with foamed plastic. This insulation also aided in preventing the formation of frost. By maintaining a continuous flow of liquid nitrogen between the walls, the test targets could be chilled to 144° K in about 80 minutes.

Leakage due to thermal shrinkage was encountered at the thermocouple lead-through point. This problem was solved by adding a pipe of such length that the end away from the chamber remained approximately at room temperature. The vacuum feed-through device was fitted at this far end. Figure 4 is a photograph of the low-temperature test fixture mounted on the end of the access chamber. The end cap seal was removed when this photograph was taken.

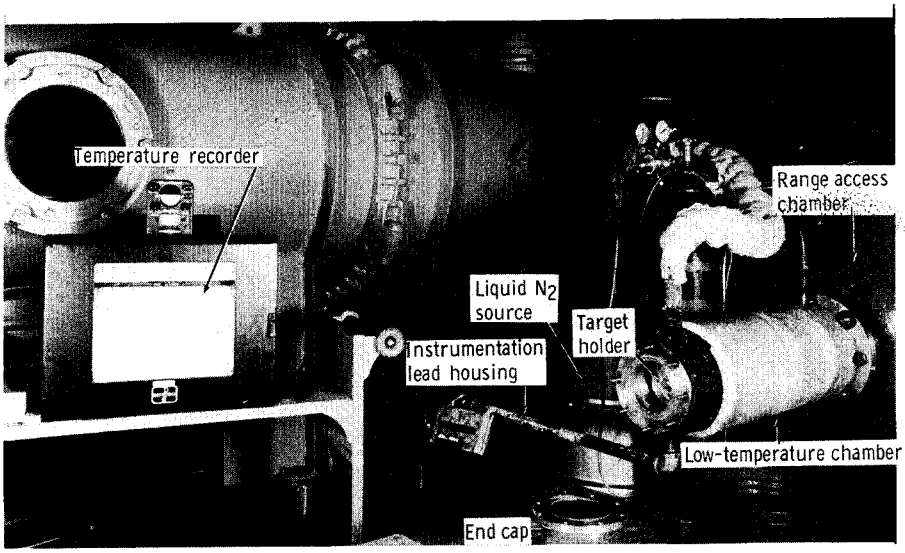

Figure 4.- Experimental arrangement for low-temperature test fixture. L-64-1595.1

Helium light-gas gun.- The helium light-gas gun shown in figure 5 consists of a 20-mm-diameter compressor tube charged with helium at a pressure of 6.9 MN/m^2 and a 5.58-mm-diameter smooth-bore launch tube which is connected to a 0.914-m-diameter vacuum chamber. A 32.4-gram powder charge was placed in the breech end of the compressor tube. The burning powder charge provided a shock front which compressed the helium gas and provided the force necessary to launch the projectile at the desired velocity. The vacuum chamber between the light-gas gun and the test chamber acted as a blast tank; the chamber also contained viewing ports to permit velocity measurements.

Velocity-measurement system.- A photograph of some of the velocity measuring instrumentation is shown in figure 6. A photographic technique was used in which two light beams are positioned 0.61 cm apart and which were directed perpendicular to the

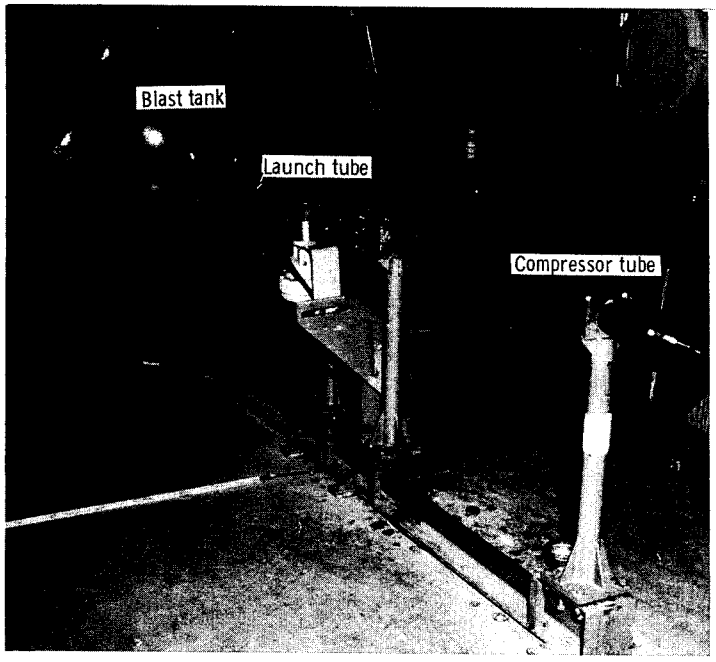

Figure 5.- Helium light-gas gun. L-64-1785.1

Figure 6.- Velocity measurement system. L-64-1786

path of the projectile. When the projectile interrupted the first light beam, a pulse from a photomultiplier tube triggered a spark gap, and a picture of the projectile was taken. Simultaneously, an interval counter was started. Similar events occurred at the second velocity measurement station, except that when the projectile arrived at this station the interval timer was stopped. The velocity was then computed from the position of the projectile, as indicated in the pictures, and the measured time interval between pictures.

PROCEDURE AND ANALYSIS

Experimental Procedure

Some preliminary experiments were conducted in both the hot- and cold-target test chambers to evaluate how well each functioned under conditions of vacuum and extreme temperature. Each chamber was capable of maintaining pressures below 5 N/m^2 at temperatures of 422° K and 144° K.

Polyethelene calibration specimens, each instrumented with an array of thermocouples, were mounted as simulated targets in each chamber to ascertain the temperature variation throughout a target. The greatest temperature difference measured on any polyethelene target was 8° K. Because the thermal diffusivity of polyethelene is approximately the same as the target materials tested (except for material E, for which no data were available), the maximum temperature difference on the actual test materials is estimated to be less than 9° K. This difference was considered to be sufficiently uniform so as not to significantly affect the data.

The general arrangement of the test apparatus is sketched in figure 1. Except for the helium-pressurized compressor tube of the light-gas gun, the entire apparatus was evacuated to a pressure of 67 N/m^2; the large size of the blast chambers made it difficult to obtain lower pressures. The system was evacuated before the targets were heated or cooled. This procedural sequence prevented the hot targets from oxidizing prior to impact and prevented the formation of frost on the surfaces of the cold target. Approximately 80 minutes were required to cool targets to a temperature of 144° K. Targets could be heated to 422° K in approximately 30 minutes.

Each of the five target materials was tested at three temperatures: 144°, 294°, and 422° K. The targets were struck with a 1.59-mm-diameter aluminum sphere traveling at a velocity of 4 km/s.

Analysis of Temperature and Material Effects

The resultant craters in these ablative materials tested were usually slender, irregular cavities, partially filled with crushed and pulverized material. Volume measurements could not be obtained from such craters with any acceptable accuracy. The

crater depths and lip diameters listed in tables III and IV were obtained by cross-sectioning the target through the crater. Some typical crater cross sections are shown in the photographs in figure 7.

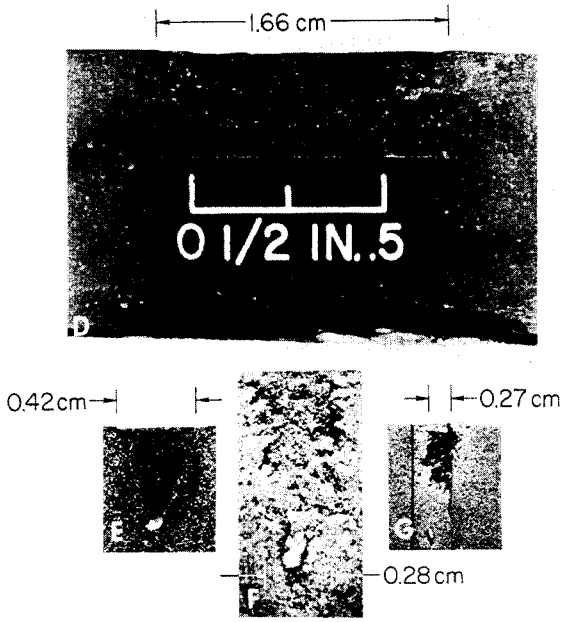

Figure 7.- Typical crater cross sections. L-66-1095

Because of the irregular nature of the craters in the ablative targets, there was difficulty in measuring the crater depths and diameters, with the result that there was a large scatter in the data. This scatter was large enough to obscure differences in damage caused by differences in temperature or material. In order to determine whether there were detectable effects due to differences in target temperature or material, a statistical analysis of the data was made. The analysis applied was that commonly known as the analysis of variance with two variables of classification; in this case the variables of classification are temperature and material. This analysis is a standard statistical technique described in most texts on statistical analysis; see, for example, reference 4.

In order to apply this method, the data are arranged first in tabular form as shown in tables III and IV. Each row contains the data for a particular temperature, while each column is associated with a particular material. Also shown in the tables is the sum of the measurements for each temperature (row) $T_{i.}$ each material (column) $T_{.j}$, the sum of all the measurements $T_{..}$, and their respective means $T_{i.}/n_i$, $T_{.j}/m_j$, and $T_{..}/N$ where n_i and m_j are the number of measurements in the row and column, respectively, and N is the total number of measurements.

An estimate of the variance (squared standard deviation) is now calculated by two different algebraic methods. The variance of either the row results SS_r or column results SS_k is estimated by the following expressions:

$$SS_r = \sum_{i=1}^{r} \frac{T_{i.}^2}{n_i} - \frac{T_{..}^2}{N} \tag{3}$$

$$SS_k = \sum_{j=1}^{k} \frac{T_{.j}^2}{m_j} - \frac{T_{..}^2}{N} \tag{4}$$

The variance SS_r is a measure of the scatter which includes both experimental scatter and variations due to temperature changes, while SS_k includes experimental scatter and material changes.

The second method of calculating the variance is given by the relationships

$$R_S = T_S - \left(SS_r + SS_k\right) \tag{5}$$

where

$$T_S = \sum_i \sum_j T_{ij}^2 - \frac{T_{..}^2}{N} \tag{6}$$

The total sum of T_S squares might be regarded as the overall variance estimated from the squared difference of each measurement from the grand mean and would include experimental scatter, temperature effects, and material effects. The residual sum of R_S squares might be the overall variance minus the variance containing temperature effects SS_r and the variance containing material effects; R_S is known as the residual sum of squares and is a measure of only the experimental scatter, without temperature or material effects. The above discussion is a rather heuristic explanation of the roles of SS_r, SS_k, and R_S. Reference should be made to standard texts on the subject for a more definitive derivation of equations (3) to (6).

The values of SS_r, SS_k, R_S, and T_S, along with the mean values of the variances $\left(R_S^*, SS_r^*, SS_k^*\right.$, see table V) are shown in table VI for the crater depth measurements and in table VII for the crater diameter measurements.

To analyze the results, the assumptions are made that: (1) there is no effect on crater sizes or depths due to changes in temperature and (2) there is no effect on crater sizes or depths due to differences in material. If these assumptions be true, the ratios SS_r^*/R_S^* and SS_k^*/R_S^* will be close to 1 and will differ from 1 only because of the scatter due to difficulties in measurement, which are assumed to be random. Both of these ratios are statistical F-ratios (they have the F-distribution which is tabulated in many texts on statistics).

If either or both of the assumptions be false, one or both of the ratios will tend to increase. Therefore, if the calculated ratios are much larger than would be expected due to chance, there is reason to doubt one or the other (or both) of the assumptions, whichever may apply. The chance value can be obtained from tables, and, in particular, a value is selected herein at the $\alpha = 0.05$ level, which means that, if the assumptions be true (the scatter is due only to randomness in measurement) the value of F at $\alpha = 0.05$ would be exceeded in only 5 percent of the cases.

RESULTS

Determination of Temperature and Material Effects

Application of the analysis-of-variance technique to the depth of penetration measurements listed in table III gives the tabulated results shown in table VI. The calculated value of the F-ratio for temperatures (F_r) is

$$F_r = \frac{SS_r^*}{R_s^*} = \frac{0.002}{0.0026} = 0.77$$

The critical value from tables of reference 5 at the 5-percent level of significance is

$$F_{r_{(.95_{cr})}}(2,8) = 4.46$$

where the first number in parentheses is the number of degrees of freedom in the numerator, and the second is the number of degrees of freedom in the denominator.

$F_{r_{(.95_{cr})}}$ should be exceeded only 5 percent of the time if there are no temperature effects. Since

$$F_r = 0.77 < F_{r_{(.95_{cr})}} = 4.46$$

there is no reason to suspect any temperature effect.

Similarly for F_k (material effects)

$$F_k = \frac{SS_k^*}{R_s^*} = \frac{0.138}{0.0026} = 53.1$$

Again, from the tables (ref. 5)

$$F_{k_{(.95_{cr})}}(4,8) = 3.84$$

Because

$$F_k = 53.1 > F_{(.95_{cr})} = 3.84$$

the hypothesis that differences in material do not cause differences in penetration was rejected.

In the same fashion the technique was applied to an analysis of the crater diameters. (See table VII.) For the temperature effects

$$F_r = \frac{0.035}{0.036} = 0.97 < F_{(.95_{cr})}(2,8) = 4.46$$

and there seems to be no detectable differences in crater diameter due to temperature effects.

However, because

$$F_k = \frac{0.793}{0.036} = 22 > F_{(.95_{cr})}(4,8) = 3.84$$

there is good reason to suspect that the different materials exhibited different amounts of damage.

Material A showed some evidence of spallation; this material had twice the density and half the target thickness of the other materials, also, the modulus of elasticity was an order of magnitude greater than the moduli of materials B to E. Because material A had characteristics so different from the others, there was some question whether the impact results on material A might be overweighing the results. To investigate this question, the analysis of variance was repeated for materials B to E, excluding material A. The results are:

For crater depths –

$$\frac{SS_r^*}{R_s^*} = 0.139 < F_{r_{(.95)}}(2,6) = 5.14$$

$$\frac{SS_k^*}{R_s^*} = 4.49 < F_{k_{(.95)}}(3,6) = 4.76$$

For crater diameters –

$$\frac{SS_r^*}{R_s^*} = 0.448 < F_{r_{(.95)}}(2,6) = 5.14$$

$$\frac{SS_k^*}{R_s^*} = 19.82 > F_{k_{(.95)}}(3,6) = 4.76$$

These calculations show that there is still a difference in crater diameter caused by material differences but that the differences in penetration depths among the materials, although large, are not large enough to conclude that the material affects the depth of penetration (at the 95-percent confidence level).

Comparison of Experiment With Established Theory

Figure 8 shows a comparison of the data obtained from this series of experiments with calculations made from the empirical equation (eq. (1)), which was determined from a lengthy series of high-velocity impacts into semi-infinite metallic and plastic targets (ref. 2). The material initial strength b was taken to be zero for plastics; the

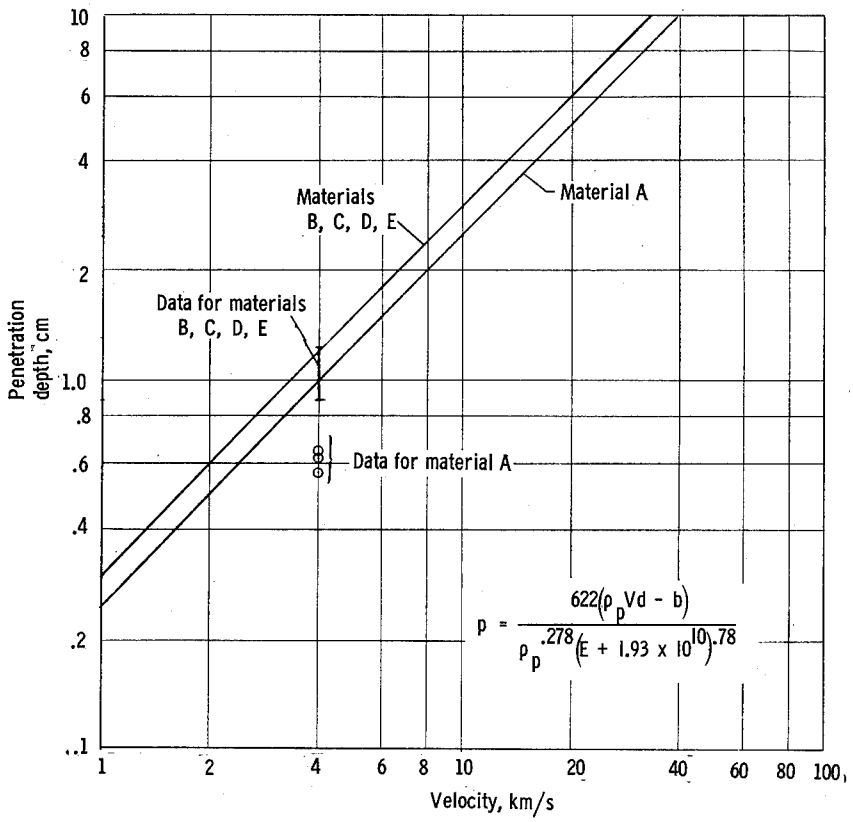

Figure 8.- Theoretical penetration as a function of velocity. The experimental data are compared with values predicted by the empirical equation (eq. (1)).

modulus E was determined from compression tests on target samples. The two straight lines represent the calculated upper and lower limits for the five materials investigated herein. The three points which deviated considerably from the band were those measured for the high-density phenolic-nylon targets in which spallation occurred from the back surface of the target material. These targets may not have conformed to the conditions under which the equation was formulated, namely, for semi-infinite targets. However, there is no reason to believe that spallation indicates a condition which would diminish the crater size.

CONCLUDING REMARKS

Five ablative target materials, consisting of high- and low-density phenolic-nylons and supported and unsupported elastomers, have been struck with 1.59-mm-diameter aluminum spheres at a velocity of 4 km/s. Two ablative target test fixtures, designed and constructed for high- and low-temperature testing, were used for impact studies at 422°, 294°, and 144° K to determine the effects of temperature and target material on the amount of cratering. The analysis-of-variance technique was applied to the data to overcome difficulties in measuring depths and diameters caused by the irregularity of the craters.

The analysis-of-variance technique indicated that there was no distinguishable difference in damage among tests at the three test temperatures, and it is concluded that, within this range of temperatures, there is little, if any, temperature effect on these materials. There is (at the 95-percent confidence level) a definite difference in the diameters of the craters among the materials. The depth of penetration into the denser phenolic-nylon target was significantly shallower than for any of the other four less dense, softer materials. The tests are considered to be inconclusive with regard to differences in the depth of penetration among the four lower density materials.

Langley Research Center,
National Aeronautics and Space Administration,
Langley Station, Hampton, Va., February 18, 1966.

REFERENCES

1. Mechtly, E. A.: The International System of Units – Physical Constants and Conversion Factors. NASA SP-7012, 1964.

2. Kinard, William H.; and Collins, Rufus D., Jr.: An Investigation of High-Velocity Impact Cratering into Nonmetallic Targets and Correlation of Penetration Data for Metallic and Nonmetallic Targets. NASA TN D-726, 1961.

3. Kinard, William H.; Lambert, C. H., Jr.; Schryer, David R.; and Casey, Francis W., Jr.: Effect of Target Thickness on Cratering and Penetration of Projectiles Impacting at Velocities to 13,000 Feet Per Second. NASA MEMO 10-18-58L, 1958.

4. Dixon, Wilfrid J.; and Massey, Frank, J., Jr.: Introduction to Statistical Analysis. Second ed., McGraw-Hill Book Co., Inc., 1957, pp. 139-145.

5. Bowker, Albert H.; and Lieberman, Gerald J.: Engineering Statistics. Prentice-Hall, Inc., c.1959.

TABLE I.- DESCRIPTION OF TARGET MATERIALS

Target	Composition	Density, ρ, km/m^3	Diameter, cm	Thickness, cm
A	High-density phenolic-nylon – 50% phenolic-resin 50% nylon powder	1150	7.62	1.70
B	Low-density phenolic-nylon – 25% phenolic-resin 50% nylon powder 25% Microballoons	580	7.62	3.38
C	Elastomer – 75% Silguard elastomer 15% Eccospheres 10% Microballoons	580	7.62	3.38
D	Elastomer supported by phenolic-honeycomb – 75% Silguard elastomer 15% Eccospheres 10% Microballoons	Honeycomb: 64 Overall: 580	7.62	3.38
E	Elastomer – 75% elastomer 15% Eccospheres 10% Microballoons	580	7.62	3.38

TABLE II.- VALUES OF ELASTIC MODULUS

Target	Elastic modulus, E, GN/m^2
A	2
B	.3
C	.03
D	.3
E	.2

TABLE III.- ANALYSIS-OF-VARIANCE TABLE FOR PENETRATION DEPTHS

	Penetration depth, cm, for material –					$T_{i.}$	$T_{i.}/n_i$
	A	B	C	D	E		
294° K (room temp.)	0.559	1.02	1.00	1.07	1.07	4.72	0.94
422° K	.610	.968	1.07	1.08	1.19	4.92	.98
134° K	.635	1.07	.899	1.10	1.17	4.87	.96
$T_{.j}$	1.804	3.06	2.97	3.25	3.43	$T_{..}$ = 14.51	
$T_{.j}/m_j$	.60	1.02	.99	1.08	1.14		$T_{..}/N$ = 0.96

TABLE IV.- ANALYSIS-OF-VARIANCE TABLE FOR CRATER DIAMETERS

	Crater diameter, cm, for material –					$T_{i.}$	$T_{i.}/n_i$
	A	B	C	D	E		
294° K (room temp.)	1.66	0.42	0.27	0.27	0.42	3.04	0.61
422° K	1.00	.40	.30	.32	.42	2.44	.49
134° K	1.80	.45	.28	.28	.36	3.17	.63
$T_{.j}$	4.46	1.27	0.85	0.87	1.20	$T_{..}$ = 8.65	
$T_{.j}/m_j$	1.49	.42	.28	.29	.40		$T_{..}/N$ = 0.58

TABLE V.- TABULATION FOR ANALYSIS OF VARIANCE

	Sum of squares	Degrees of freedom	Mean square
Row means	SS_r	r - 1	$SS_r^* = \frac{SS_r}{(r - 1)}$
Column means	SS_k	k - 1	$SS_k^* = \frac{SS_k}{(k - 1)}$
Residual	R_S	(r - 1)(k - 1)	$R_S^* = \frac{R_S}{(r - 1)(k - 1)}$
Total	T_S	rk - 1	

TABLE VI.- ANALYSIS OF VARIANCE FOR CRATER DEPTHS

	Sum of squares	Degrees of freedom	Mean square
Row means (temperature)	0.004	2	0.002
Column means (material)	.553	4	.138
Residual	.021	8	.0026
Total	.578	14	

TABLE VII.- ANALYSIS OF VARIANCE FOR CRATER DIAMETERS

	Sum of squares	Degrees of freedom	Mean square
Row means (temperature)	0.07	2	0.035
Column means (material)	3.17	4	.793
Residual	.29	8	.036
Total	3.53	14	

NASA-Langley, 1966 L-4173

"The aeronautical and space activities of the United States shall be conducted so as to contribute . . . to the expansion of human knowledge of phenomena in the atmosphere and space. The Administration shall provide for the widest practicable and appropriate dissemination of information concerning its activities and the results thereof."

—NATIONAL AERONAUTICS AND SPACE ACT OF 1958

NASA SCIENTIFIC AND TECHNICAL PUBLICATIONS

TECHNICAL REPORTS: Scientific and technical information considered important, complete, and a lasting contribution to existing knowledge.

TECHNICAL NOTES: Information less broad in scope but nevertheless of importance as a contribution to existing knowledge.

TECHNICAL MEMORANDUMS: Information receiving limited distribution because of preliminary data, security classification, or other reasons.

CONTRACTOR REPORTS: Technical information generated in connection with a NASA contract or grant and released under NASA auspices.

TECHNICAL TRANSLATIONS: Information published in a foreign language considered to merit NASA distribution in English.

TECHNICAL REPRINTS: Information derived from NASA activities and initially published in the form of journal articles.

SPECIAL PUBLICATIONS: Information derived from or of value to NASA activities but not necessarily reporting the results of individual NASA-programmed scientific efforts. Publications include conference proceedings, monographs, data compilations, handbooks, sourcebooks, and special bibliographies.

Details on the availability of these publications may be obtained from:

SCIENTIFIC AND TECHNICAL INFORMATION DIVISION

NATIONAL AERONAUTICS AND SPACE ADMINISTRATION

Washington, D.C. 20546